Journal of Neuroscience Methods 408 (2024) 110171

Contents lists available at ScienceDirect

Journal of Neuroscience Methods

journal homepage: www.elsevier.com/locate/jneumeth

Large field-of-view metabolic profiling of murine brain tissue following morphine incubation using label-free multiphoton microscopy

Carlos A. Renteria [a,b], Jaena Park [a,b], Chi Zhang [a], Janet E. Sorrells [a,b], Rishyashring R. Iyer [a,c], Kayvan F. Tehrani [a], Alejandro De la Cadena [a], Stephen A. Boppart [a,b,c,d,e,*]

[a] Beckman Institute for Advanced Science and Technology, University of Illinois Urbana-Champaign, Urbana, IL, USA
[b] Department of Bioengineering, University of Illinois Urbana-Champaign, Urbana, IL, USA
[c] Department of Electrical and Computer Engineering, University of Illinois Urbana-Champaign, Urbana, IL, USA
[d] Neuroscience Program, University of Illinois Urbana-Champaign, Urbana, IL, USA
[e] NIH/NIBIB P41 Center for Label-free Imaging and Multiscale Biophotonics (CLIMB), University of Illinois Urbana-Champaign, Urbana, IL, USA

ARTICLE INFO

Keywords:
Multiphoton microscopy
Morphine
Nonlinear optics
Label-free imaging
Metabolism

ABSTRACT

Background: Although the effects on neural activation and glucose consumption caused by opiates such as morphine are known, the metabolic machinery underlying opioid use and misuse is not fully explored. Multiphoton microscopy (MPM) techniques have been developed for optical imaging at high spatial resolution. Despite the increased use of MPM for neural imaging, the use of intrinsic optical contrast has seen minimal use in neuroscience.

New Method: We present a label-free, multimodal microscopy technique for metabolic profiling of murine brain tissue following incubation with morphine sulfate (MSO_4). We evaluate two- and three-photon excited autofluorescence, and second and third harmonic generation to determine meaningful intrinsic contrast mechanisms in brain tissue using simultaneous label-free, autofluorescence multi-harmonic (SLAM) microscopy.

Results: Regional differences quantified in the cortex, caudate, and thalamus of the brain demonstrate region-specific changes to metabolic profiles measured from FAD intensity, along with brain-wide quantification. While the overall intensity of FAD signal significantly decreased after morphine incubation, this metabolic molecule accumulated near the nucleus accumbens.

Comparison with existing methods: Histopathology requires tissue fixation and staining to determine cell type and morphology, lacking information about cellular metabolism. Tools such as fMRI or PET imaging have been widely used, but lack cellular resolution. SLAM microscopy obviates the need for tissue preparation, permitting immediate use and imaging of tissue with subcellular resolution in its native environment.

Conclusions: This study demonstrates the utility of SLAM microscopy for label-free investigations of neural metabolism, especially the intensity changes in FAD autofluorescence and structural morphology from third-harmonic generation.

1. Introduction

Neural activation and communication are metabolically demanding processes that require glucose to facilitate cellular metabolism. The brain splits metabolic function between cell types: neurons are primarily oxidative in nature, and astrocytes primarily glycolytic in nature (Magistretti and Allaman, 2015). The underlying metabolic machinery is critical to facilitate neural activation, as aberrances to this machinery could result in insufficient ATP generation to facilitate neural activation. Thus, elucidating the metabolic pathways in the brain is crucial for investigating the effects of pharmaceutical drugs, environmental toxins, neural byproducts such as amyloid-β, and other toxins on neural metabolism as well as neural activity. One such agent, morphine, is a common opiate used to relieve pain, and poses high risk for addiction. Its abuse has increased substantially over time (Volkow et al., 2019), with estimates of over a hundred thousand opioid-related deaths reported in 2021, according to data from the Center for Disease Control and Prevention (CDC) (Spencer et al., 2023). Critical to addressing this problem

* Corresponding author at: Beckman Institute for Advanced Science and Technology, University of Illinois Urbana-Champaign, Urbana, IL, USA.
E-mail address: boppart@illinois.edu (S.A. Boppart).

https://doi.org/10.1016/j.jneumeth.2024.110171
Received 21 January 2024; Received in revised form 15 April 2024; Accepted 17 May 2024
Available online 21 May 2024

is understanding how morphine, other opiates, and broadly other drugs affect neural metabolism across scales. This requires technologies that can monitor cellular metabolism across the molecular scale.

Molecular metabolic brain activity has traditionally been investigated with Positron Emission Tomography (PET). This is an imaging technique that makes use of a biocompatible radioisotope that is intravenously injected into patients and used to quantify relative metabolism in the brain (Berti et al., 2011). Magnetic resonance imaging (MRI) has also emerged as a tool to do this, using methods that measure tissue oxygenation to measure brain activity (Heeger and Ress, 2002) on the whole-brain scale. Unfortunately, these modalities lack the spatial resolution needed to identify biochemical and structural changes at a sub-cellular scale. In hospital settings, histology typically fills this void—a technique to visualize cellular structures and their microenvironment to diagnose pathologies. Although histology is a laborious and time-consuming technique (Bryant et al., 2019), it effectively provides cellular and molecular resolution. However, it sacrifices functional information. Despite the extensive knowledge of the effect of morphine on the brain through MRI and PET imaging techniques, our understanding of how it affects the local neural microenvironment is limited. Technologies that can bridge these gaps to provide metabolic information at the molecular scale in living tissue are critical.

A solution to the drawbacks of PET and MRI is multiphoton microscopy (MPM). MPM has seen a dramatic increase in its utility for molecular neuroscience research in the past two decades. Notably, two-photon microscopy has become more popular due to the narrow axial confinement of emitted fluorescence mediated through two-photon absorption (Larson, 2011; Denk et al., 1990; Benninger and Piston, 2013). This results in a higher signal-to-noise ratio (SNR) in targeted structures due to minimized out-of-focus fluorescence excitation. Additionally, the use of near-infrared (NIR) excitation light facilitates deep-tissue imaging and prevents photodamage compared to visible light sources (Benninger and Piston, 2013), (Tischbirek et al., 2015). These advantages have also been leveraged to realize various investigations into neural circuitry by simultaneously imaging and manipulating neurons (Yang et al., 2018; Packer et al., 2015; Liu et al., 2020) by stimulation with single-cell resolution using optogenetics (Oron et al., 2012; Prakash et al., 2012; Rickgauer and Tank, 2009). These physical parameters become more advantageous with three-photon absorption because it enables imaging at further increased depths of up to 1–2 mm (Ouzounov et al., 2017; Wang and Xu, 2020; Wang et al., 2020).

Despite the increased use of MPM for metabolic imaging, a substantial number of these studies in neuroscience have been limited to the use of calcium and voltage indicators for imaging neural soma and dendritic spines (Russell et al., 2022; Accanto et al., 2023; Adam et al., 2019; Yang et al., 2016; Zhang et al., 2018; Pan and Gan, 2008), techniques that require genetic manipulation or the addition of exogenous indicators for imaging neuronal activity. While these emissive labels enable a plethora of applications, there are a variety of intrinsic fluorophores and harmonophores present at the molecular scale that can be easily exploited for label-free optical microscopy (Xu et al., 1996a), (Xu et al., 1996b). These include NAD(P)H, FAD, and many others (Xu et al., 1996a, 1996b; Katz and Robison, 2002; Yan et al., 2023; Skala et al., 2007), which can be interrogated at 1110 nm with three-photon excited autofluorescence (3PAF, NAD(P)H) and two-photon excited autofluorescence (2PAF, FAD) (Tu et al., 2016), (Tu et al., 2017). The notation for NAD(P)H includes both phosphorylated (NADPH) and unphosphorylated (NADH) forms of NAD(P)H, which both fluoresce. The fluorescent coenzymes NAD(P)H and FAD in particular are important due to their central roles in cellular metabolism, exchanging electrons to facilitate several processes in oxidative phosphorylation and glycolysis (Georgakoudi and Quinn, 2023).

Furthermore, there are molecular structures, such as collagen, that have nonlinear optical properties that promote frequency doubling of incident light (Campagnola, 2011), (Chen et al., 2012). Structural interfaces, such as those between bilipid cellular membranes, lipid droplets, and water, enable frequency tripling of the excitation sources (Weigelin et al., 2016). Known as second and third harmonic generation (SHG and THG), respectively, these contrasts reveal the structure of the local microenvironment.

Leveraging these nonlinear signals, we recently introduced a novel imaging technique known as simultaneous label-free autofluorescence multi-harmonic (SLAM) microscopy. The SLAM microscope is an imaging platform that not only reveals the tissue microenvironment with unprecedented detail, but also provides quantitative morpho-functional information of native tissue. Previous investigations using this technology have shown notable changes in the tumor microenvironment, including levels and organization of collagenous structures in tumors (You et al., 2018a, 2018b, 2019), vesicular shuttling in and around tumors (You et al., 2019), and quantification of the NAD(P)H and FAD levels in cancerous tissue to determine metabolic changes in the tumor microenvironment (You et al., 2021) using the relative intensities of NAD(P)H, FAD, and the ratio of their intensities.

Due to the limited number of available tools for metabolic, molecular imaging of neural tissue, investigations relating to neural metabolism in intact tissue at the cellular level are rare. In addition to imaging calcium dynamics and histological visualization of excised brain tissue, it is important to determine the molecular metabolism in neural tissue. This information is crucial not only for understanding the etiology and pathogenesis of neural disease, but also for identifying the metabolic effects in the brain following chemical exposure. One of the most prominent technologies for measuring neural metabolism at this scale is two-photon microscopy using intrinsic optical metabolic optical signatures, notably NAD(P)H and FAD (Georgakoudi and Quinn, 2023), (Kolenc and Quinn, 2019). As these biomolecules are directly implicated in cellular metabolism, they give a direct and label-free method for identifying cellular metabolism, which was previously been used to identify metabolic shuttling between neurons and astrocytes (Kasischke et al., 2004). Fluorescence lifetime imaging microscopy (FLIM) makes extended use of the decay characteristics of these intrinsic fluorophores as an added form of contrast, which is also used to quantify and separate biomolecular species in neural imaging (Yaseen et al., 2013), (Chia et al., 2008). Although these methods are commonly used for direct imaging of metabolic information in different cell types, nonlinear structural contrast from THG and SHG cannot be easily measured using the ~750 nm sources typically used for these investigations. How and the extent to which these contrast methods can be combined for comprehensive profiling of the neural microenvironment remains underexplored.

Here, we demonstrate the utility of SLAM microscopy for metabolic profiling of neural (murine brain) tissue following incubation with morphine sulfate. Mosaics of harvested murine brain slices were collected to quantify, at a large field-of-view, NAD(P)H and FAD levels, as well as THG signal throughout a segment of brain tissue with and without morphine sulfate—a depressant of neural metabolic activity (London, 1990)—to determine its effect on NAD(P)H and FAD levels in different brain regions. THG intensity was quantified and correlated between channels to determine its relationship to both structural and metabolic information in this study. We found an overall decrease in FAD levels throughout the brain, which correlated strongly with THG. NAD(P)H signal was too low for quantification in this investigation, suggesting low concentration and collection efficiency of the co-enzyme in brain tissue.

2. Methods

2.1. Experimental setup

For this investigation, we used a custom-made SLAM microscope (You et al., 2018a). Briefly, the output of a femtosecond fiber laser centered at 1030 nm, a 20 MHz repetition rate, and 3.34 W output (Satsuma, Amplitude) was directed to a photonic crystal fiber (PCF,

LMA-PM-15, NKT Photonics) for supercontinuum generation. Undesired portions of the spectra were blocked, and the spectral band at 1110 ± 30 nm was used for excitation. Pulses were compressed to near their transform-limit (~35 fs) by addition of group delay dispersion to compensate for dispersion of the fiber and optical setup using a commercial pulse shaper (MIIPS Box 640, BiophotonicSolutions). The laser beam was raster scanned across the sample using a pair of computer-controlled galvanometer-mounted mirrors. The autofluorescence and multi-harmonic generation signals were detected simultaneously from four photon-counting photomultiplier tubes (PMTs, H7421–40, Hamamatsu), with filters at 365–375 nm (THG), 420–480 nm (NAD(P)H), 540–570 nm (SHG), and 580–640 nm (FAD). Each 400×400 pixel field-of-view (FOV) spanned 600×600 μm, with a 12.5 μs pixel dwell time, well below levels that may otherwise cause thermal damage (Picot et al., 2018). The wider field-of-view images were acquired by translating the harvested brain slice on a motorized 3-axis stage to collect multiple tiles, which were then combined to create large FOV mosaic images for subsequent analysis. Images were pseudo-colored yellow for 2PAF, cyan for 3PAF, green for SHG, and magenta for THG.

2.2. Sample preparation

All animal experiments were conducted in accordance with the relevant guidelines and regulations in a protocol approved by the Institutional Animal Care and Use Committee (IACUC) at the University of Illinois Urbana-Champaign. All experiments were performed on fresh brain tissue, without prior fixation or other chemical preparation. C57BL/6 mice were euthanized by decapitation following isoflurane inoculation and the whole brain was immediately harvested from each mouse. Thereafter, the brain was placed on ice and transferred to an ice-cooled vibratome filled with cutting solution (in mM, 2.5 KCl, 1.25 NaH_2PO_4, 10 $MgCl_2$, 0.5 $CaCl_2$, 234 Sucrose, 11 Glucose, 26 $NaHCO_3$) for slice preparation. The brains were sliced coronally to 300 μm thick slices, and immediately placed in artificial cerebrospinal fluid (aCSF) (in mM, 2.5 KCl, 10 Glucose, 126 NaCl, 26 $NaHCO_3$, 1.25 NaH_2PO_4, 2 $MgCl_2$, 2 $CaCl_2$) at room temperature. The control slices were placed on a clean microscope cover glass on the sample stage immediately. The morphine-treated slices were placed in a separate container for holding until imaged. Treated slices were incubated at room temperature with different concentrations (20 μM and 40 μM) of morphine-sulfate (MSO_4, Sigma Aldrich, M8777) for at least 20 minutes, then imaged. A total of n = 9 brain slices from N = 2 mice were used in analysis for this investigation. A total of 4 control slices, 4 slices exposed to 20 μM of MSO_4, and 1 slice exposed to 40 μM of MSO_4 were used.

2.3. Image analysis

Images were analyzed using a custom MATLAB script. Superpixels for each SLAM channel were generated by down sampling the original images into the median values of 25×25 pixel tiles. A median filter was used to reduce the contribution of outliers on pixel values, providing a better representation of the anticipated pixel value in a given area. Due to the large amount of low-intensity pixels that biased any statistical analysis, all pixels with zero photons were omitted from analysis. This serves to both generate pixels representative of the true values within a given region of an image, and to reduce data quantity for increased computational efficiency. Furthermore, data was processed such that pixels within the 25th to 75th percentile were used for analysis, removing contributions from outliers. Raw images were used for visualization of brain data. Thereafter, for brain-wide analysis, the superpixels from all relevant channels were extracted for further statistical analysis and visualization. Due to the large number of pixels used for statistical analysis, effect size provided a more accurate account of the magnitude of differences between experimental groups. A Cohen's D effect size metric was used to quantify the magnitude of differences between conditions, with effect sizes below −1 or above 1 considered significant in this work. For regional analyses, a region of interest (ROI) was manually drawn around the cortex, caudate, and thalamus. Treatment conditions were then compared based on region.

3. Results

3.1. Label-free metabolic profiling of brain tissue

Fig. 1 shows representative SLAM mosaics from two adjacent brain slices without and with morphine treatment (Fig. 1A, F), along with zoomed-in individual images from the hippocampus of the imaged brain slices (Fig. 1B-E, and Fig. 1G-J) highlighted in red boxes. Each individual box shows molecular and structural information from 2PAF (Fig. 1B and G), 3PAF (Fig. 1C and H), SHG (Fig. 1D and I), and THG (Fig. 1E and J). The 2PAF signal shows several bright structures (representative sites highlighted with red arrows in Fig. 1B and G), which in this context, are neural cells and their processes, similar to previous imaging of FAD in brain tissue (Chen et al., 2021). While the 3PAF and SHG signals for both tissues are faint, they reveal some structures. These structures, however, appear to coincide with the much brighter structures in the 2PAF images, suggesting that, for native tissue, these are 2PAF signals seeping into other channels. The THG channel has bright signals in these tissues due to the strong contrast in refractive index between larger neural bodies, axons, processes, and other fibrous structures. THG signal is generated most profoundly near lipids, and consequently cell membranes due to their high nonlinear coefficient χ^3 that governs THG generation and partial phase-matching conditions posed from focusing the laser source near dendrites in brain tissue (Witte et al., 2011). This supports the strong THG signal we see from dendrites, axons, and white-matter tracts, which have many highly lipidic structures, such as myelin sheaths. These contrasts qualitatively show the rich structural and biochemical information from endogenous fluorophores and harmonophores in brain tissue revealed by SLAM microscopy.

Beyond qualitative information, the imaging data acquired can be used to quantify the biochemical information obtained using SLAM microscopy. Fig. 2A shows another representative image of a brain slice imaged with SLAM, and the signals from our 2PAF, 3PAF, SHG, and THG channels in each local region in a FOV (Fig. 2B) and for the whole-brain (Fig. 2C). Each imaging modality provides a distinct form of contrast, which promotes visualization of different structures. The THG modality is especially useful for structural imaging, showing distinct morphological characteristics unique to each brain region due to the interfaces between structures, especially lipids and fibrous structures like dendrites (Witte et al., 2011), that are accentuated by the THG contrast. The 2PAF and 3PAF channels show fluorescence primarily from FAD and NAD(P)H respectively, among other intrinsic fluorophores (Croce and Bottiroli, 2014), which provides a conduit for neural metabolism. The SHG channel provides information from highly fibrillary structures, such as collagen, which is not a prominent component of brain tissues (Novak and Kaye, 2000). Consequently, very little SHG signal is seen in the brain (Esquibel et al., 2020). This SHG channel was omitted from quantification and analysis in this study. Surprisingly, little NAD(P)H signal was present in this data. Because the brain is such a metabolically demanding organ (Magistretti and Allaman, 2015), we initially anticipated much larger NAD(P)H signals from our samples. This is consistent with the results previously shown by our group (Iyer et al., 2022) and others, with concentrations as low as 60 μM measured in human brain tissue (Zhu et al., 2015), suggesting inherently low levels of NAD(P)H in brain tissue. This could further be exacerbated by the reduced probability of three-photon fluorescence of NAD(P)H in this window due to its cubic dependence on laser power (Tu et al., 2016), (Tu et al., 2017), (You et al., 2018a), (Boyd, 2008), along with its low nonlinear cross-sections for two and three-photon absorption (Xu et al., 1996b). Finally, since neuronal cells have larger surface areas than epithelial cells arising from their numerous projections within which NADH could

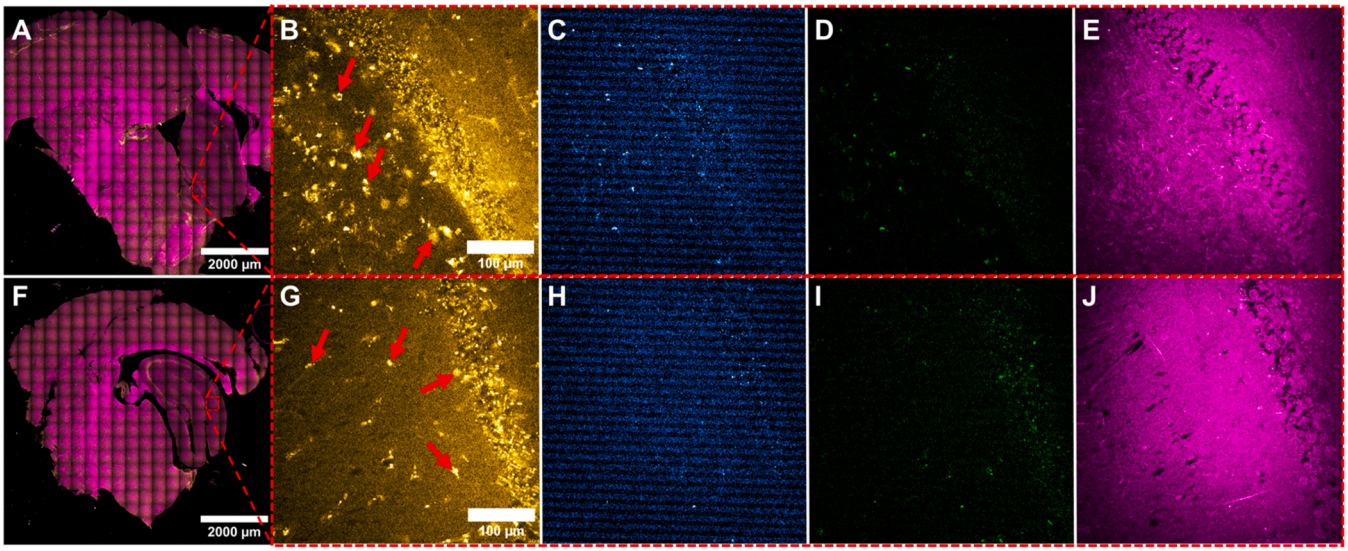

Fig. 1. Label-free images of brain tissue acquired using SLAM microscopy. (A) Mosaicked image of all autofluorescence channels from an untreated murine brain slice. (B-E) 2PAF, 3PAF, SHG, and THG channels, respectively, for the brain slice in (A). (F) Adjacent brain slice treated with 20 μM MSO_4. (G-J) Corresponding 2PAF, 3PAF, SHG, and THG images, respectively. Red arrows point to bright-yellow structures, which are likely to be neurons in this channel.

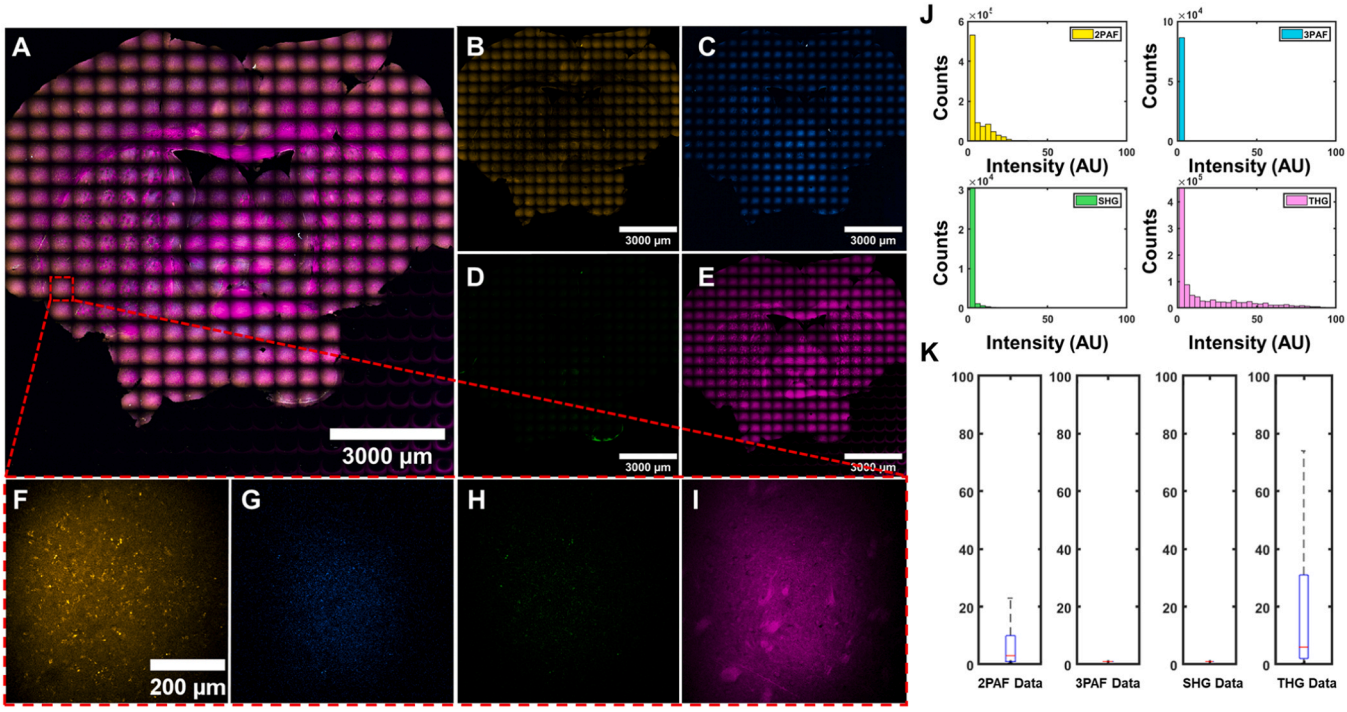

Fig. 2. SLAM images of brain tissue for all channels, and quantification of dynamic range for all data used in this investigation. (A) Brain-slice and data from SLAM microscopy datasets. (B-E) Whole-slice mosaics from 2PAF (B), 3PAF (C), SHG (D), and THG (E) channels. (F-I) Montage with individual 2PAF (F), 3PAF (G), SHG (H), and THG (I) for individual mosaics and for whole-brain tissue. (J) Histogram for all SLAM microscopy data captured from each individual channel from numerous brain tissue. (K) Box-and-whisker plot illustrating the distribution of individual SLAM channels for brain tissue collected in this investigation. Statistics generated from n = 9 slices from N = 2 mice.

be distributed, the NADH levels within each pixel are likely to be lower. A combination of these factors causes low NAD(P)H signals in brain tissue with SLAM. Histograms and box plots representing the distribution for all modalities across the images used in this study are shown in Fig. 2J and K, respectively. These results emphasize the wide distribution of FAD and THG signals captured using SLAM, channels that reveal neuronal bodies and interfaces, respectively. Additionally, this data demonstrates that SHG and NAD(P)H signals produce negligible contributions—for which both channels were omitted from subsequent analysis in this work, as no meaningful statistics can be quantified from such a narrow distribution. Collectively, these modalities provide rich molecular and structural information, which enables rapid metabolic profiling of the specimen.

3.2. Brain-wide profiling of morphine incubation

Superpixel intensities (median of 25×25 pixels as defined in Section 2.3), were compared between control and morphine-treated brain slices for the whole brain slice in the 2PAF and 3PAF channels. Fig. 3A-3 C shows representative SLAM images of the specific whole-brain slices from FAD, while Fig. 3D-F show the NAD(P)H counterparts used for quantification. Note that Figs. 3A and 3D are from the control, Figs. 3B and 3E from the sample incubated with 20 μM of morphine sulfate, and Figs. 3C and 3F from the sample incubated with 40 μM of morphine sulfate. The NAD(P)H channels are shown for completeness (Fig. 3G, blue histogram), however, quantification is not performed on this channel due to the low 3PAF signal mentioned previously. Fig. 3G, yellow histogram, shows the relative FAD distributions between the experimental conditions from the same imaging session. This consisted of three adjacent slices from one mouse brain. There is a noticeably larger increase in FAD intensities (Fig. 3H), which is more pronounced following the 40 μM exposure. This could be related to an overall increase in molecular machinery performing oxidative phosphorylation, and an increase in glycolysis (Walsh et al., 2016), (Walsh et al., 2014). These results demonstrate the capabilities of SLAM microscopy to acquire multimodal images from a mouse whole-brain slice to infer information about its structure and metabolic processes.

3.3. Regional quantification of metabolic imaging

One benefit of acquiring large field-of-view mosaics using SLAM is the ability to monitor and analyze local changes in the tissue microenvironment. This is especially important for neural imaging, where different brain regions are responsible for different tasks. Monitoring energy demands using the label-free fluorophores present in the brain can inform on the local metabolic energy demands. The cortex, caudate, and larger thalamic regions, which includes the nucleus accumbens, are annotated in Supplementary Fig. 1. To quantify local differences in the FAD intensity, a region of interest was drawn in each individual region, and further quantified before and after morphine incubation, as in Section 3.2. For the same dataset shown in Fig. 3, changes are seen throughout brain regions consistent with the brain-wide analysis. Fig. 4A-C shows the distribution of the NAD(P)H and FAD intensities in the cortex (Fig. 4A), caudate (Fig. 4B), and thalamus (Fig. 4C). Corresponding box and whisker plots are illustrated in Fig. 4D-F. Notably, all regions showed a consistent increase in mean intensity following incubation, which is also represented in the histogram by an overall decrease in low pixel intensities and larger distribution of higher intensities. This change in histogram shape suggests pixel-to-pixel changes in intensity increase to the FAD levels rather than a large change in a few selected pixels, or previously zero pixels suddenly increasing in intensity. These dynamics between conditions suggest increased oxidative phosphorylation, leading to increased glycolysis, which would result in increased FAD (Kolenc and Quinn, 2019), (Hu et al., 2020).

The nucleus accumbens is a region implicated in drug addiction due to its role in processing pleasure, reward, and motivation (Salgado and Kaplitt, 2015) among other characteristics in mammals. Therefore, this specific region was targeted for metabolic comparisons between morphine treated and untreated brain slices (Figs. 4C and 4F). Histogram and box plots show a notable increase in the mean FAD signal and distribution compared to the untreated conditions. This is consistent with the other brain regions, and is especially profound after incubation with 40 μM morphine sulfate.

3.4. Brain-wide statistical profiling of morphine incubation

Lastly, the FAD level intensities between multiple control and morphine-treated conditions were analyzed to determine the net effect of morphine incubation on neural metabolism for all brain tissue harvested in this study. To that end, Fig. 5A shows a summary of the distributions of FAD intensities between untreated (control) and all morphine-treated conditions. Fig. 5B shows a bar graph to compare the means between control and morphine-treated conditions, and Fig. 5C a box and whisker plots to illustrate the underlying distribution of FAD intensities between conditions. The compiled data in Figs. 5B and 5C do not exhibit statistically significant decreases in FAD intensities in all morphine-treated conditions, compared to controls. When separated by concentration, the trends change to show an overall decrease in FAD levels at 40 μM than 20 μM, as shown in Fig. 5 E and F. In fact, consideration of the distribution of intensities for all data in Fig. 5D shows a flattening of higher intensity pixels compared to lower intensity pixels, reflective of the results from the bar and box plots. It is possible for the results in Figs. 3 and 4, notably the difference in FAD trends, to be

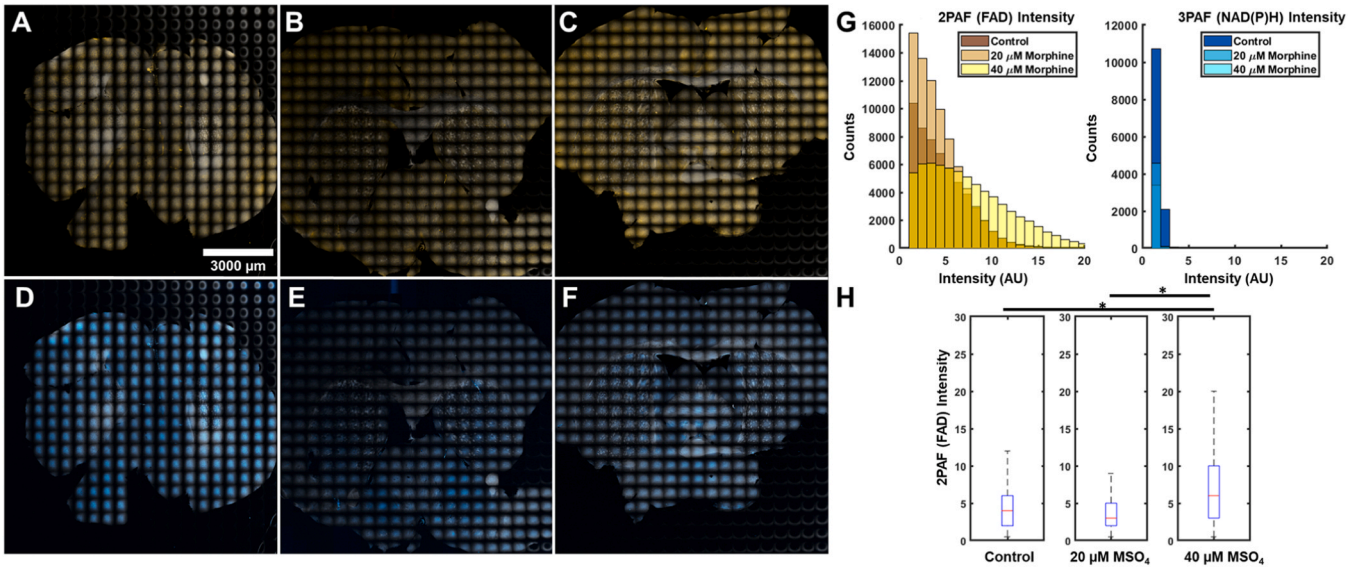

Fig. 3. Brain-wide quantification of FAD and NAD(P)H. Isolated FAD channels from tissue incubated in (A) control aCSF, (B) 20 μM morphine sulfate, and (C) 40 μM morphine sulfate. (D-F) NAD(P)H channels that correspond to the FAD channels between (A-C). (G) Histograms for the FAD and NAD(P)H channels for the data in (A-F), and (H) the box and whisker plots for the FAD data in each condition. * denotes $p < 0.01$ and Cohen's D below −1 or above 1. Statistics from n = 3 slices from N = 1 mouse.

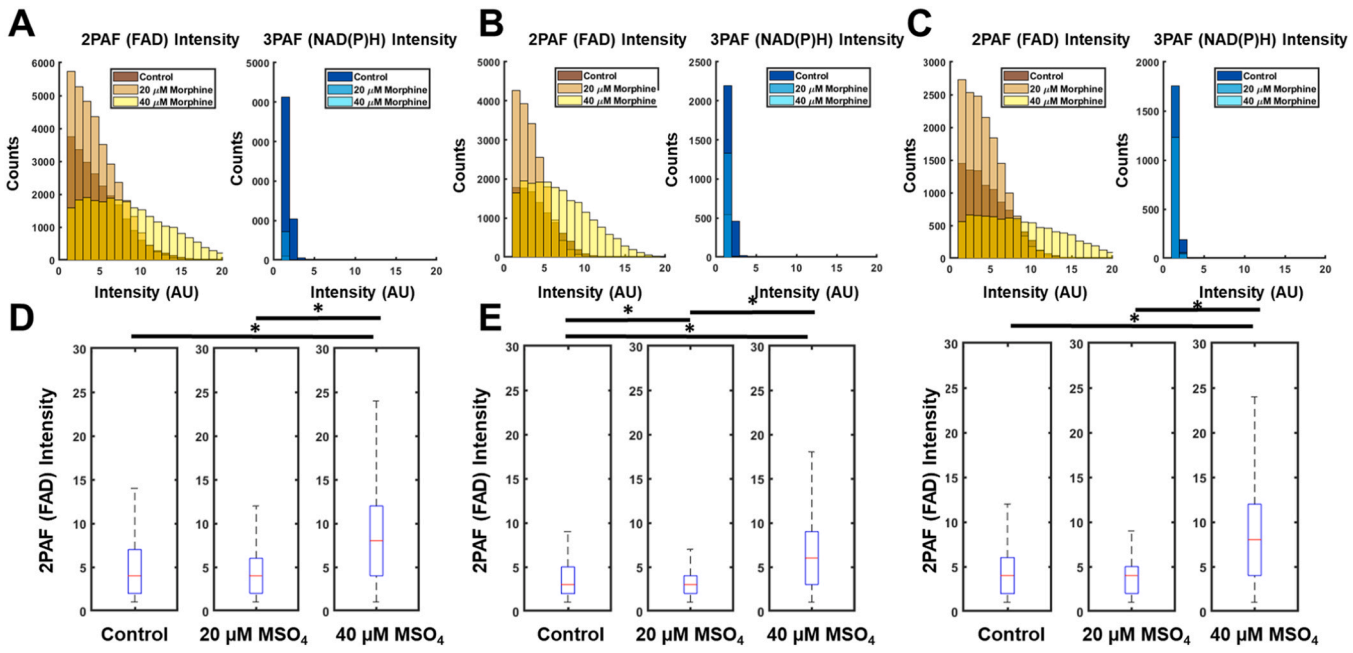

Fig. 4. Results for data from Fig. 3 separated by cortex (A, D), caudate (B, E) and thalamus (C, F). Notably, histograms of the 2PAF and 3PAF data (A-C) and corresponding box and whisker plot (D-F). * denotes $p < 0.01$ and Cohen's D below −1 or above 1. Statistics generated from n = 3 slices (one control, one 20 μM, and one 40 μM slice) from N=1 mouse.

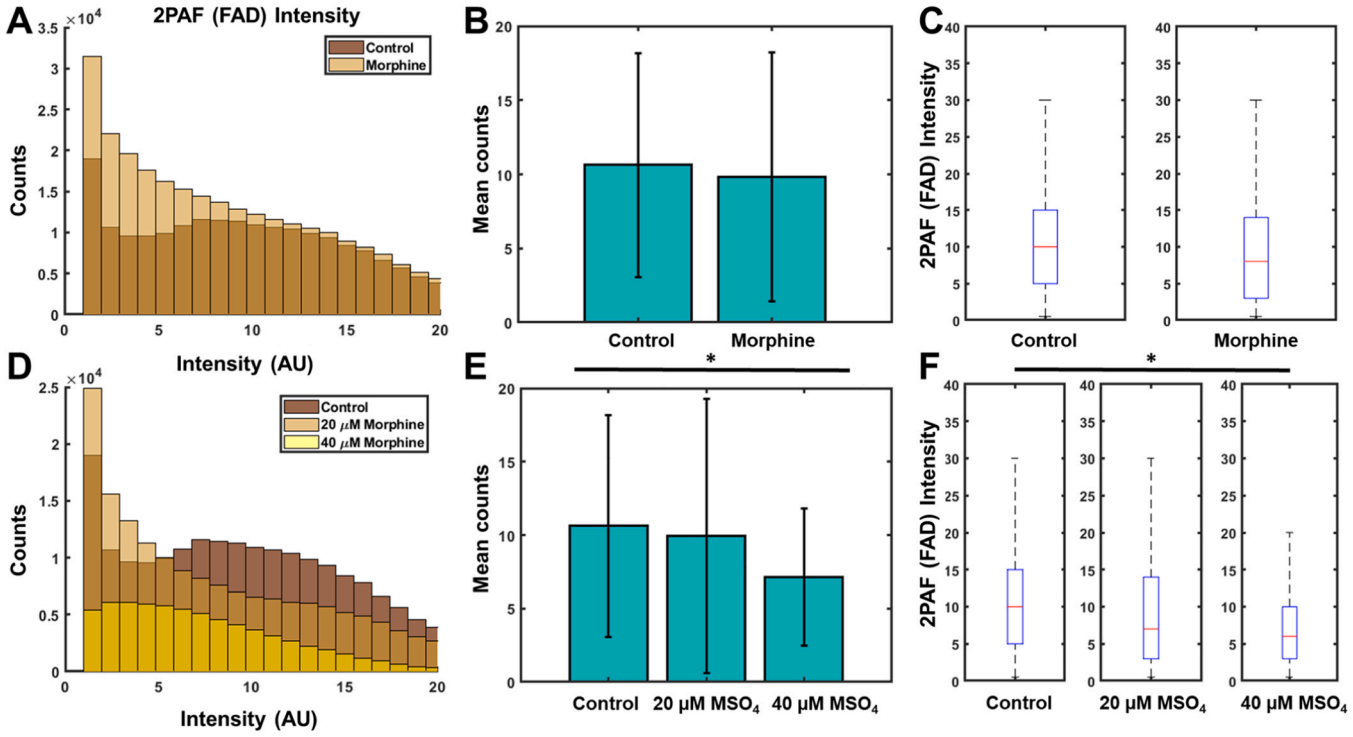

Fig. 5. Whole-brain statistics for treated and untreated brain tissue. The results in this figure summarize data from all datasets captured in this study. (A) Histogram comparing 2PAF of FAD between control and morphine-treated samples. (B) Bar plots illustrating mean 2PAF of untreated (n = 210,915 pixels) and treated (n = 284,744 pixels) conditions, and (C) corresponding box-and whisker plot. (D) Histogram, (E) bar graph, and (F) box-and-whisker plot separated by control (n = 210,915 pixels), 20 μM treatment (n = 181,510 pixels), and 40 μM (n = 67,576 pixels) morphine treatment. Error bars +/- standard mean error (S.E.M). * denotes $p < 0.01$ and Cohen's D below −1 or above 1. Statistics generated from n = 4 control slices, n = 4 slices exposed to 20 μM MSO_4, and n = 1 slice exposed to 40 μM MSO_4, from N = 2 mice.

attributed to inherent variability between mice, while the overall trends not necessarily tracking with that mouse. These results illustrate the utility of SLAM microscopy for comparing overall trends in neural metabolism between experimental conditions.

4. Discussion

4.1. Implications of SLAM microscopy for neural metabolic imaging

Given that many studies suggest that astrocytes are particularly sensitive to morphine (Slezak et al., 2013), our findings imply that the changes observed in FAD signal could be primarily from astrocytes, an argument that would also be consistent with the hypothesis for astrocytes as the primary mediators of neural metabolism (Mächler et al., 2016). In this context, the decrease in FAD levels throughout excised brain slices observed in this work is attributable to an overall reduction in glycolysis through the involvement of FAD in the electron transport chain (ETC) in cells (Georgakoudi and Quinn, 2023) through fatty acid metabolism (Ahmad et al., 2023). This FAD reduction is consistent with studies showing decreased glucose utilization throughout the brain in human patients following morphine administration (London, 1990). In contrast, the data from the nucleus accumbens and adjacent brain regions showed increased FAD levels, suggesting an increased glycolytic activity at these specific sites, a finding that is supported by other studies that show an increase in expression for genes associated with astrocyte glycolysis following morphine treatment in astrocytes (Rao et al., 2023).

Interestingly, additional results showed that along with the decreases in FAD intensities following morphine incubation came decreases in THG intensity as well (Supplementary Fig. 2). Moreover, this trend goes beyond aggregate changes that track with those of FAD. Correlation coefficients between different channels for all datasets shown here (Supplementary Fig. 3) show that, between THG and FAD, there appears to be a strong correlation between these channels, especially compared to others (Supplementary table 1), despite at times showing clear differences in apparent structures (Figs. 1 and 2). We attribute this partially to an overlap in structures, but this would not necessarily explain why there is a correlation between the intensities of signals from the correlation coefficients. Lipids have a higher probability of invoking THG (Witte et al., 2011). It is possible that changes in lipid content during cellular metabolism following morphine incubation track with the changes in FAD, and thus overall cellular energy metabolism. Additional work on these modalities and metabolites would need to be pursued to determine if this is a consistent phenomenon, identify pathways invoked from these changes, and determine if this trend is consistent. Lastly, *in vivo* studies can be performed to assess if the results from brain tissue coincide with changes in neural metabolism in living mice.

The results from this study validate the use of SLAM microscopy for rapid visualization and quantification of large field-of-view cellular metabolism in fresh brain slices. This offers a strong complement to histology for identifying pathologies from excised tissue, and an intermediate morphological solution to quantify cellular metabolism at higher resolution than PET and MRI.

4.2. Limitations and future directions

Label-free metabolic imaging at the molecular scale is currently minimally pursued in neural imaging. These results and prior studies have demonstrated that quantification of NAD(P)H in particular remains a challenge for three-photon fluorescence in label-free neural imaging (Iyer et al., 2022), (Zhu et al., 2015). While acquisition of three-photon autofluorescence is possible, the NAD(P)H signals are often incredibly small compared to those of two-photon FAD and THG. In general, low photon counts are observed for many biomolecules in most multiphoton systems (Driscoll et al., 2011). In our study, this is likely because of the combination of low NAD(P)H signals in the brain, along with the reduced efficiency of three photon absorption that results in even weaker signals. These features are much more prominent in cancer, epithelial, kidney, liver, extracellular vesicles, and other non-neural tissues previously investigated with this microscopy system (Tu et al., 2016), (Tu et al., 2017), (You et al., 2018a), (You et al., 2018b), (Park et al., 2023; Tehrani et al., 2023; Yang et al., 2022). Future microscope designs can leverage lower repetition rates to increase peak power (De La Cadena et al., 2024), and the likelihood of these rarer multiphoton events, at the expense of slower imaging speeds (Tu et al., 2016), (You et al., 2018a). More sensitive photodetectors, such as hybrid photodetectors, could also be used to increase system sensitivity to otherwise low signals (Sorrells et al., 2022). Other quantitative approaches, such as fluorescence lifetime imaging (Bower et al., 2021), (Becker et al., 2004), (Becker, 2012), which has been demonstrated to help distinguish between NAD(P)H and its different isoforms *in vivo* in the cerebral cortex (Yaseen et al., 2017), and vibrational microscopy techniques (Vanna et al., 2022; Ji et al., 2018; Mrđenović et al., 2024), can also bridge this gap.

Despite the ability to resolve single-cells, SLAM microscopy alone is unable to differentiate between astrocytes and other glial cells to interrogate this hypothesis. Investigating this requires tags specific to each cell type, and few label-free approaches demonstrate sufficient sensitivity to distinguish between neural cell types. Previous work in our group, however, has demonstrated the capability of differentiating neurons from astrocytes following glutamate administration using NAD(P)H transients (Bower et al., 2021). The combination of multiple MPM imaging modalities and temporal changes is an active area of research, which could circumvent this limitation in the local microenvironment to help answer questions relating to neuron-astrocyte communication and metabolism. Additionally, red-shifted tags to differentiate each cell type could be used for such studies, which would minimize crosstalk with FAD or NAD(P)H autofluorescence.

4.3. Advantages and disadvantages of a single 1110-nm source for metabolic neural imaging

Contrasts from specific nonlinear optical processes, notably from second harmonic generation and three-photon fluorescence of NAD(P)H, are inherently low in brain tissue, making it challenging to use these for evaluating neural morphology and metabolism. This is due to the lack of harmonophores in the brain, such as collagen, that would produce SHG, and the combination of the decreased three-photon absorption probability and low-concentration of NAD(P)H in the brain relative to other tissues. Previous and ongoing work in our group has evaluated the use of two-photon absorption using light centered around 750 nm to quantify NAD(P)H and FAD, along with FLIM as a method for expanding the suitability of this approach. While SLAM microscopy provides an ideal window to adequately resolve multiple forms of structural and metabolic contrast, especially since many photodetectors and microscope objectives used for multiphoton microscopy are optimized for collecting visible light, there is an inherent trade-off when imaging brain tissue specifically because of these factors. Similarly, while ~750–800 nm sources are ideal for metabolic imaging of FAD and NAD(P)H (Skala et al., 2007), (Georgakoudi and Quinn, 2023), (Kolenc and Quinn, 2019), (Yaseen et al., 2013), (Chia et al., 2008), structural imaging using THG is lost since deep UV light is generated from this process, which does not penetrate very deep in tissue. As harmonophores are not densely populated in the brain, SHG is low, regardless of the source.

This does, however, provide a window of opportunity to combine label-free imaging with other commonly implemented tools, such as calcium imaging, to compare fluctuations in calcium imaging to those from the metabolites investigated in this study (Bower et al., 2021), (Díaz-García et al., 2021). This can be expanded to astrocytes and other glia cells as well, along with the use of other labels to expand the wealth of information available to researchers. Additionally, if a tunable source is used that can switch between 1110 nm and 750 nm, the benefits of each of these tools can be combined when used sequentially to provide structural information from the former, and metabolic information with the latter. This information may not be able to be gathered simultaneously, but as structural information does not change rapidly in neural tissue, an imaging paradigm can be designed to switch between

contrasts as needed during experimentation. This is an area where SLAM excels, as the 1110 nm wavelength is optimal for generating signal from each of these nonlinear contrasts for simultaneous detection, which accelerates imaging speed and enables spatial and temporal co-registration between the different channels. As neural imaging is trending towards longer wavelengths for deeper tissue imaging, (Ouzounov et al., 2017; Wang and Xu, 2020; Wang et al., 2020) this also offers a better alternative to 750 nm due to the increased depth penetration offered by 1110 nm.

5. Conclusion

SLAM microscopy was used for label-free, molecular-scale, metabolic profiling of excised brain tissue slices treated with morphine-sulfate or untreated. Our results demonstrate differences in FAD signals between treated and untreated conditions following exposure. Full brain-slice and regional brain-slice analysis was performed by selecting distinct brain regions of interest, notably the cortex, caudate, and thalamus. The relative FAD levels were then quantified by region. We analyzed the intensities of NAD(P)H, FAD, SHG, and THG signals in the brain, and determined that the FAD and THG channels consistently provide strong signal and contrast in brain tissue. These promote high-SNR metabolic and structural neural imaging, respectively. Although there is interest in measuring intensities of NAD(P)H, their intensities are far too low, which makes it less reliable for quantification in brain tissue. This is attributed to low NAD(P)H levels present in the brain, and the reduced efficiency of three-photon absorption at 1110 nm for NAD(P)H, which is known to have very small nonlinear cross-sections compared to other fluorophores.

Overall, we demonstrate SLAM microscopy for metabolic profiling of brain tissue, and highlight areas of improvement for the next generation of label-free multiphoton systems for studying the brain molecular, metabolic, and structural microenvironment. These include using lower repetition rate lasers, using more sensitive photodetectors to improve SNR from samples with low photon count rates, and combining these imaging techniques with modulation transfer techniques (e.g., lock-in or box-car detection) to improve image SNR and imaging speed.

CRediT authorship contribution statement

Janet E. Sorrells: Writing – review & editing, Conceptualization. **Chi Zhang:** Writing – review & editing, Methodology, Investigation, Conceptualization. **Kayvan F. Tehrani:** Writing – review & editing, Supervision. **Rishyashring R. Iyer:** Writing – review & editing, Conceptualization. **Carlos Renteria:** Writing – review & editing, Writing – original draft, Visualization, Validation, Project administration, Methodology, Investigation, Formal analysis, Conceptualization. **Jaena Park:** Writing – review & editing, Methodology, Investigation, Conceptualization. **Stephen A. Boppart:** Writing – review & editing, Supervision, Resources, Project administration, Investigation, Funding acquisition, Conceptualization. **Alejandro De la Cadena:** Writing – review & editing.

Declaration of Competing Interest

S.A.B. is co-founder of LiveBx, LLC, and K.F.T. is founder of Eleuthra Photonics, Inc., which are commercializing the imaging technologies developed in this study. S.A.B. and K.F.T. have disclosed intellectual property related to multiphoton imaging. All remaining authors declare no competing interests.

Data availability

Data will be made available on request, and through a collaborative research agreement.

Acknowledgement

The authors would like to thank Dr. Edita Aksamitiene and Eric Chaney for protocol management, and Darold Spillman for administrative assistance. Research reported in this publication was supported by training grants from the National Institute of Biomedical Imaging and Bioengineering (NIBIB) and the National Institutes of Environmental Health Sciences (NIEHS) of the NIH under Award Numbers T32EB019944 and T32ES007326. The content is solely the responsibility of the authors and does not necessarily represent the official views of the National Institutes of Health. This research was also supported in part by grants from the Air Force Office of Scientific Research (FA9550–17–1–0387) and the NIH/NIBIB Center for Label-free Imaging and Multiscale Biophotonics (CLIMB) (P41EB031772). Additional information can be found at http://biophotonics.illinois.edu.

Appendix A. Supporting information

Supplementary data associated with this article can be found in the online version at doi:10.1016/j.jneumeth.2024.110171.

References

Accanto, N., et al., 2023. A flexible two-photon fiberscope for fast activity imaging and precise optogenetic photostimulation of neurons in freely moving mice (Jan.). Neuron vol. 111 (2), 176–189. https://doi.org/10.1016/j.neuron.2022.10.030.

Adam, Y., et al., May 2019. Voltage imaging and optogenetics reveal behaviour-dependent changes in hippocampal dynamics. Nature vol. 569 (7756), 413–417. https://doi.org/10.1038/s41586-019-1166-7.

Ahmad, M., Wolberg, A., Kahwaji, C.I., 2023. " in *StatPearls*, Treasure Island (FL). Biochemistry, Electron Transport Chain. StatPearls Publishing. Accessed: Dec. 19, 2023. [Online]. Available: ⟨http://www.ncbi.nlm.nih.gov/books/NBK526105/⟩.

Becker, W., 2012. Fluorescence lifetime imaging – techniques and applications," (Aug.), vol. 247 (2), 119–136. https://doi.org/10.1111/j.1365-2818.2012.03618.x.

Becker, W., Bergmann, A., Hink, M.A., König, K., Benndorf, K., Biskup, C., 2004. Fluorescence lifetime imaging by time-correlated single-photon counting (Jan.). Microsc. Res. Tech. vol. 63 (1), 58–66. https://doi.org/10.1002/jemt.10421.

Benninger, R.K.P., Piston, D.W., 2013. Two-photon excitation microscopy for the study of living cells and tissues (Jun.). Curr. Protoc. Cell Biol. vol. 59 (1). https://doi.org/10.1002/0471143030.cb0411s59.

Berti, V., Pupi, A., Mosconi, L., 2011. PET/CT in diagnosis of dementia (Jun.). Ann. N. Y. Acad. Sci. vol. 1228 (1), 81–92. https://doi.org/10.1111/j.1749-6632.2011.06015.x.

Bower, A.J., Renteria, C., Li, J., Marjanovic, M., Barkalifa, R., Boppart, S.A., 2021. High-speed label-free two-photon fluorescence microscopy of metabolic transients during neuronal activity (Feb.). Appl. Phys. Lett. vol. 118 (8), 081104. https://doi.org/10.1063/5.0031348.

Boyd, R.W., 2008. Optically Induced Damage and Multiphoton Absorption. in Nonlinear Optics. Elsevier, pp. 543–560. https://doi.org/10.1016/B978-0-12-369470-6.00012-5.

Bryant, P., Haine, N., Johnston, J., Ntiamoah, P., 2019. Application of large format tissue processing in the histology laboratory (Jul.). J. Histotechnol. vol. 42 (3), 150–162. https://doi.org/10.1080/01478885.2019.1628425.

Campagnola, P., 2011. Second harmonic generation imaging microscopy: applications to diseases diagnostics (May). Anal. Chem. vol. 83 (9), 3224–3231. https://doi.org/10.1021/ac1032325.

Chen, D., et al., 2021. Label-free imaging of human brain tissue at subcellular resolution for potential rapid intra-operative assessment of glioma surgery. Theranostics vol. 11 (15), 7222–7234. https://doi.org/10.7150/thno.59244.

Chen, X., Nadiarynkh, O., Plotnikov, S., Campagnola, P.J., 2012. Second harmonic generation microscopy for quantitative analysis of collagen fibrillar structure (Apr.). Nat. Protoc. vol. 7 (4), 654–669. https://doi.org/10.1038/nprot.2012.009.

Chia, T.H., Williamson, A., Spencer, D.D., Levene, M.J., 2008. Multiphoton fluorescence lifetime imaging of intrinsic fluorescence in human and rat brain tissue reveals spatially distinct NADH binding (Mar.). Opt. Express vol. 16 (6), 4237. https://doi.org/10.1364/OE.16.004237.

Croce, A.C., Bottiroli, G., 2014. Autofluorescence spectroscopy and imaging: a tool for biomedical research and diagnosis (Dec.). Eur. J. Histochem.. https://doi.org/10.4081/ejh.2014.2461.

De La Cadena, A., Park, J., Tehrani, K.F., Renteria, C.A., Monroy, G.L., Boppart, S.A., 2024. Simultaneous label-free autofluorescence multi-harmonic microscopy driven by the supercontinuum generated from a bulk nonlinear crystal (Feb). Biomed. Opt. Express vol. 15 (2), 491. https://doi.org/10.1364/BOE.504832.

Denk, W., Strickler, J.H., Webb, W.W., 1990. Two-photon laser scanning fluorescence microscopy (Apr.). Science vol. 248 (4951), 73–76. https://doi.org/10.1126/science.2321027.

Díaz-García, C.M., Meyer, D.J., Nathwani, N., Rahman, M., Martínez-François, J.R., Yellen, G., 2021. The distinct roles of calcium in rapid control of neuronal glycolysis

and the tricarboxylic acid cycle (Feb.). eLife vol. 10, e64821. https://doi.org/10.7554/eLife.64821.
Driscoll, J.D., et al., 2011. Photon counting, censor corrections, and lifetime imaging for improved detection in two-photon microscopy (Jun.). J. Neurophysiol. vol. 105 (6), 3106–3113. https://doi.org/10.1152/jn.00649.2010.
Esquibel, C.R., et al., 2020. Second harmonic generation imaging of collagen in chronically implantable electrodes in brain tissue (Jul.). Front. Neurosci. vol. 14, 95. https://doi.org/10.3389/fnins.2020.00095.
Georgakoudi, I., Quinn, K.P., 2023. Label-free optical metabolic imaging in cells and tissues (Jun.). Annu. Rev. Biomed. Eng. vol. 25 (1), 413–443. https://doi.org/10.1146/annurev-bioeng-071516-044730.
Heeger, D.J., Ress, D., 2002. What does fMRI tell us about neuronal activity? (Feb.). Nat. Rev. Neurosci. vol. 3 (2), 142–151. https://doi.org/10.1038/nrn730.
Hu, L., Wang, N., Cardona, E., Walsh, A.J., 2020. Fluorescence intensity and lifetime redox ratios detect metabolic perturbations in T cells (Oct.). Biomed. Opt. Express vol. 11 (10), 5674. https://doi.org/10.1364/BOE.401935.
Iyer, R.R., et al., 2022. Tracking the binding of multi-functional fluorescent tags for Alzheimer's disease using quantitative multiphoton microscopy," (Sep.). J. Biophotonics vol. 15 (9), e202200105. https://doi.org/10.1002/jbio.202200105.
Ji, M., et al., 2018. Label-free imaging of amyloid plaques in Alzheimer's disease with stimulated Raman scattering microscopy (Nov.). Sci. Adv. vol. 4 (11), eaat7715. https://doi.org/10.1126/sciadv.aat7715.
Kasischke, K.A., Vishwasrao, H.D., Fisher, P.J., Zipfel, W.R., Webb, W.W., 2004. Neural activity triggers neuronal oxidative metabolism followed by astrocytic glycolysis (Jul.). Science vol. 305 (5680), 99–103. https://doi.org/10.1126/science.1096485.
Katz, M.L., Robison, W.G., 2002. What is lipofuscin? Defining characteristics and differentiation from other autofluorescent lysosomal storage bodies (May). Arch. Gerontol. Geriatr. vol. 34 (3), 169–184. https://doi.org/10.1016/S0167-4943(02)00005-5.
Kolenc, O.I., Quinn, K.P., 2019. Evaluating cell metabolism through autofluorescence imaging of NAD(P)H and FAD (Feb.). Antioxid. Redox Signal. vol. 30 (6), 875–889. https://doi.org/10.1089/ars.2017.7451.
Larson, A.M., 2011. Multiphoton microscopy (Jan.). Nat. Photonics vol. 5 (1). https://doi.org/10.1038/nphoton.an.2010.2.
Liu, Y.-Z., et al., 2020. Simultaneous two-photon activation and imaging of neural activity based on spectral–temporal modulation of supercontinuum light (Nov.). Neurophotonics vol. 7 (04). https://doi.org/10.1117/1.NPh.7.4.045007.
London, E.D., 1990. Morphine-induced metabolic changes in human brain: studies with positron emission tomography and [Fluorine 18]fluorodeoxyglucose (Jan.). Arch. Gen. Psychiatry vol. 47 (1), 73. https://doi.org/10.1001/archpsyc.1990.01810130075010.
Mächler, P., et al., 2016. *In Vivo* evidence for a lactate gradient from astrocytes to neurons (Jan.). Cell Metab. vol. 23 (1), 94–102. https://doi.org/10.1016/j.cmet.2015.10.010.
Magistretti, P.J., Allaman, I., 2015. A cellular perspective on brain energy metabolism and functional imaging (May). Neuron vol. 86 (4), 883–901. https://doi.org/10.1016/j.neuron.2015.03.035.
Mrđenović, D., Combes, B.F., Ni, R., Zenobi, R., Kumar, N., 2024. Probing chemical complexity of amyloid plaques in Alzheimer's disease mice using hyperspectral raman imaging (Jan.). ACS Chem. Neurosci. vol. 15 (1), 78–85. https://doi.org/10.1021/acschemneuro.3c00607.
Novak, U., Kaye, A.H., 2000. Extracellular matrix and the brain: components and function (Jul.). J. Clin. Neurosci. vol. 7 (4), 280–290. https://doi.org/10.1054/jocn.1999.0212.
Oron, D., Papagiakoumou, E., Anselmi, F., Emiliani, V., 2012. Two-photon optogenetics. In: in *Progress in Brain Research*, vol. 196. Elsevier, pp. 119–143. https://doi.org/10.1016/B978-0-444-59426-6.00007-0.
Ouzounov, D.G., et al., 2017. *In vivo* three-photon imaging of activity of GCaMP6-labeled neurons deep in intact mouse brain (Apr.). Nat. Methods vol. 14 (4), 388–390. https://doi.org/10.1038/nmeth.4183.
Packer, A.M., Russell, L.E., Dalgleish, H.W.P., Häusser, M., 2015. Simultaneous all-optical manipulation and recording of neural circuit activity with cellular resolution *in vivo* (Feb.). Nat. Methods vol. 12 (2), 140–146. https://doi.org/10.1038/nmeth.3217.
Pan, F., Gan, W., 2008. Two-photon imaging of dendritic spine development in the mouse cortex (May). Dev. Neurobiol. vol. 68 (6), 771–778. https://doi.org/10.1002/dneu.20630.
Park, J., et al., Sep. 2023. *In vivo* label-free optical signatures of chemotherapy response in human pancreatic ductal adenocarcinoma patient-derived xenografts. Commun. Biol. vol. 6 (1), 980. https://doi.org/10.1038/s42003-023-05368-y.
Picot, A., et al., 2018. Temperature rise under two-photon optogenetic brain stimulation (Jul.). Cell Rep. vol. 24 (5), 1243–1253.e5. https://doi.org/10.1016/j.celrep.2018.06.119.
Prakash, R., et al., 2012. Two-photon optogenetic toolbox for fast inhibition, excitation and bistable modulation (Dec.). Nat. Methods vol. 9 (12), 1171–1179. https://doi.org/10.1038/nmeth.2215.
Rao, J., Sun, W., Wang, X., Li, J., Zhang, Z., Zhou, F., 2023. A novel role for astrocytic fragmented mitochondria in regulating morphine addiction (Oct.). Brain. Behav. Immun. vol. 113, 328–339. https://doi.org/10.1016/j.bbi.2023.07.030.
Rickgauer, J.P., Tank, D.W., 2009. Two-photon excitation of channelrhodopsin-2 at saturation (Sep.). Proc. Natl. Acad. Sci. vol. 106 (35), 15025–15030. https://doi.org/10.1073/pnas.0907084106.
Russell, L.E., et al., 2022. All-optical interrogation of neural circuits in behaving mice (Jul.). Nat. Protoc. vol. 17 (7), 1579–1620. https://doi.org/10.1038/s41596-022-00691-w.
Salgado, S., Kaplitt, M.G., 2015. The nucleus accumbens: a comprehensive review. Stereotact. Funct. Neurosurg. vol. 93 (2), 75–93. https://doi.org/10.1159/000368279.
Skala, M.C., et al., 2007. *In vivo* multiphoton microscopy of NADH and FAD redox states, fluorescence lifetimes, and cellular morphology in precancerous epithelia (Dec.). Proc. Natl. Acad. Sci. vol. 104 (49), 19494–19499. https://doi.org/10.1073/pnas.0708425104.
Slezak, M., et al., 2013. Astrocytes are a neural target of morphine action via glucocorticoid receptor-dependent signaling (Apr.). Glia vol. 61 (4), 623–635. https://doi.org/10.1002/glia.22460.
Sorrells, J.E., et al., 2022. Computational photon counting using multithreshold peak detection for fast fluorescence lifetime imaging microscopy (Aug.). ACS Photonics vol. 9 (8), 2748–2755. https://doi.org/10.1021/acsphotonics.2c00505.
M. Spencer *et al.*, "Estimates of Drug Overdose Deaths involving Fentanyl, Methamphetamine, Cocaine, Heroin, and Oxycodone: United States, 2021," National Center for Health Statistics (U.S.), May 2023. doi: 10.15620/cdc:125504.
Tehrani, K.F., Park, J., Chaney, E.J., Tu, H., Boppart, S.A., 2023. Nonlinear imaging histopathology: a pipeline to correlate gold-standard hematoxylin and eosin staining with modern nonlinear microscopy (Jul.). IEEE J. Sel. Top. Quantum Electron. vol. 29 (4: Biophotonics), 1–8. https://doi.org/10.1109/JSTQE.2022.3233523.
Tischbirek, C., Birkner, A., Jia, H., Sakmann, B., Konnerth, A., 2015. Deep two-photon brain imaging with a red-shifted fluorometric Ca $^{2+}$ indicator (Sep.). Proc. Natl. Acad. Sci. vol. 112 (36), 11377–11382. https://doi.org/10.1073/pnas.1514209112.
Tu, H., et al., 2016. Stain-free histopathology by programmable supercontinuum pulses (Aug.). Nat. Photonics vol. 10 (8), 534–540. https://doi.org/10.1038/nphoton.2016.94.
Tu, H., et al., 2017. Concurrence of extracellular vesicle enrichment and metabolic switch visualized label-free in the tumor microenvironment (Jan.). Sci. Adv. vol. 3 (1), e1600675. https://doi.org/10.1126/sciadv.1600675.
Vanna, R., et al., 2022. Vibrational imaging for label-free cancer diagnosis and classification (Feb.). Riv. Nuovo Cim. vol. 45 (2), 107–187. https://doi.org/10.1007/s40766-021-00027-6.
Volkow, N.D., Jones, E.B., Einstein, E.B., Wargo, E.M., 2019. Prevention and treatment of opioid misuse and addiction: a review (Feb.). JAMA Psychiatry vol. 76 (2), 208. https://doi.org/10.1001/jamapsychiatry.2018.3126.
Walsh, A.J., et al., 2014. Quantitative optical imaging of primary tumor organoid metabolism predicts drug response in breast cancer (Sep.). Cancer Res vol. 74 (18), 5184–5194. https://doi.org/10.1158/0008-5472.CAN-14-0663.
Walsh, A.J., Castellanos, J.A., Nagathihalli, N.S., Merchant, N.B., Skala, M.C., 2016. Optical imaging of drug-induced metabolism changes in murine and human pancreatic cancer organoids reveals heterogeneous drug response (Jul.). Pancreas vol. 45 (6), 863–869. https://doi.org/10.1097/MPA.0000000000000543.
Wang, T., et al., 2020. Quantitative analysis of 1300-nm three-photon calcium imaging in the mouse brain (Jan.). eLife vol. 9, e53205. https://doi.org/10.7554/eLife.53205.
Wang, T., Xu, C., 2020. Three-photon neuronal imaging in deep mouse brain (Aug.). Optica vol. 7 (8), 947. https://doi.org/10.1364/OPTICA.395825.
Weigelin, B., Bakker, G.-J., Friedl, P., 2016. Third harmonic generation microscopy of cells and tissue organization (Jan.). J. Cell Sci., jcs.152272. https://doi.org/10.1242/jcs.152272.
Witte, S., et al., 2011. Label-free live brain imaging and targeted patching with third-harmonic generation microscopy (Apr.). Proc. Natl. Acad. Sci. vol. 108 (15), 5970–5975. https://doi.org/10.1073/pnas.1018743108.
Xu, C., Williams, R.M., Zipfel, W., Webb, W.W., 1996b. Multiphoton excitation cross-sections of molecular fluorophores (Sep.). Bioimaging vol. 4 (3), 198–207. https://doi.org/10.1002/1361-6374(199609)4:3<198::AID-BIO10>3.0.CO;2-X.
Xu, C., Zipfel, W., Shear, J.B., Williams, R.M., Webb, W.W., 1996a. Multiphoton fluorescence excitation: new spectral windows for biological nonlinear microscopy (Oct.). Proc. Natl. Acad. Sci. vol. 93 (20), 10763–10768. https://doi.org/10.1073/pnas.93.20.10763.
Yan, Y., et al., 2023. Fluorescence intensity and lifetime imaging of lipofuscin-like autofluorescence for label-free predicting clinical drug response in cancer (Feb.). Redox Biol. vol. 59, 102578. https://doi.org/10.1016/j.redox.2022.102578.
Yang, L., et al., 2022. Label-free multimodal nonlinear optical imaging of needle biopsy cores for intraoperative cancer diagnosis (May). J. Biomed. Opt. vol. 27 (05). https://doi.org/10.1117/1.JBO.27.5.056504.
Yang, W., Carrillo-Reid, L., Bando, Y., Peterka, D.S., Yuste, R., 2018. Simultaneous two-photon imaging and two-photon optogenetics of cortical circuits in three dimensions (Feb.). eLife vol. 7, e32671. https://doi.org/10.7554/eLife.32671.
Yang, H.H., St-Pierre, F., Sun, X., Ding, X., Lin, M.Z., Clandinin, T.R., 2016. Subcellular imaging of voltage and calcium signals reveals neural processing *in vivo* (Jun.). Cell vol. 166 (1), 245–257. https://doi.org/10.1016/j.cell.2016.05.031.
Yaseen, M.A., et al., 2017. Fluorescence lifetime microscopy of NADH distinguishes alterations in cerebral metabolism *in vivo* (May). Biomed. Opt. Express vol. 8 (5), 2368. https://doi.org/10.1364/BOE.8.002368.
Yaseen, M.A., Sakadžić, S., Wu, W., Becker, W., Kasischke, K.A., Boas, D.A., 2013. *In vivo* imaging of cerebral energy metabolism with two-photon fluorescence lifetime microscopy of NADH (Feb.). Biomed. Opt. Express vol. 4 (2), 307. https://doi.org/10.1364/BOE.4.000307.
You, S., et al., 2018b. Slide-free virtual histochemistry (Part II): detection of field cancerization (Nov.). Biomed. Opt. Express vol. 9 (11), 5253. https://doi.org/10.1364/BOE.9.005253.
You, S., et al., 2018a. Intravital imaging by simultaneous label-free autofluorescence-multiharmonic microscopy (May). Nat. Commun. vol. 9 (1), 2125. https://doi.org/10.1038/s41467-018-04470-8.

You, S., et al., 2019. Label-free visualization and characterization of extracellular vesicles in breast cancer (Nov.). Proc. Natl. Acad. Sci. vol. 116 (48), 24012–24018. https://doi.org/10.1073/pnas.1909243116.

You, S., Chaney, E.J., Tu, H., Sun, Y., Sinha, S., Boppart, S.A., 2021. Label-free deep profiling of the tumor microenvironment (May). Cancer Res vol. 81 (9), 2534–2544. https://doi.org/10.1158/0008-5472.CAN-20-3124.

Zhang, Z., Russell, L.E., Packer, A.M., Gauld, O.M., Häusser, M., 2018. Closed-loop all-optical interrogation of neural circuits *in vivo* (Dec.). Nat. Methods vol. 15 (12), 1037–1040. https://doi.org/10.1038/s41592-018-0183-z.

Zhu, X.-H., Lu, M., Lee, B.-Y., Ugurbil, K., Chen, W., 2015. *In vivo* NAD assay reveals the intracellular NAD contents and redox state in healthy human brain and their age dependences (Mar.). Proc. Natl. Acad. Sci. vol. 112 (9), 2876–2881. https://doi.org/10.1073/pnas.1417921112.